

# Contact-mediated cellular communication supplements positional information to regulate spatial patterning during development

Chandrashekar Kuyyamudi,<sup>1,2</sup> Shakti N. Menon,<sup>1</sup> and Sitabhra Sinha<sup>1,2</sup>

<sup>1</sup>*The Institute of Mathematical Sciences, CIT Campus, Taramani, Chennai 600113, India*

<sup>2</sup>*Homi Bhabha National Institute, Anushaktinagar, Mumbai 400 094, India*

(Dated: January 25, 2021)

Development in multi-cellular organisms is marked by a high degree of spatial organization of the cells attaining distinct fates in the embryo. We show that receptor-ligand interaction between cells in close physical proximity adaptively regulates the local process of selective gene expression in the presence of a global field set up by a diffusing morphogen that provides positional cues. This allows information from the cellular neighborhood to be incorporated into the emergent thresholds of morphogen concentration that dictate cell fate, consistent with recent experiments.

Spatial symmetry breaking is a fundamental prerequisite to morphogenesis, or the development of form, in living organisms, such that an initially homogeneous domain exhibits patterns in the concentrations of molecular species referred to as morphogens [1–4]. This can come about through either self-organizing reaction-diffusion processes [5–7] or from the anisotropy associated with the concentration gradient of a morphogen produced by a localized source [8–10]. While in the simplest scenario involving the latter mechanism, the morphogen diffuses through space subject to uniform linear degradation [11–15], more complex means of establishing a morphogen gradient have been proposed [16–21]. Cells attain different fates according to the positional information provided by the local concentration of the morphogen vis-a-vis threshold values that emerge from the dynamics of the interpretation module of their genetic regulatory network [22–25]. However, the spatial pattern of cell fates is not entirely determined by these local interactions as recent experiments have highlighted the role of cell-cell communication in this process [26].

Cells in the developing embryo are known to interact with other cells that are in close physical proximity through contact-mediated signaling. This can occur through binding between membrane-bound receptors and ligands on the surfaces of neighboring cells, a prominent example being the evolutionarily conserved Notch signaling pathway [27]. Notch-mediated interactions, that are believed to have arisen early in evolution, have been shown to play a crucial role in the development of all metazoans [27, 28]. It has been demonstrated to help sharpen the boundaries between regions having different cell fates in the presence of fluctuating morphogen concentrations [29], providing an important mechanism for systems to be robust with respect to noisy signals [30–32]. More importantly, Notch signaling is capable of self-regulation as the signaling between neighboring cells implements an effective feedback loop [33].

In this paper we present a plausible mechanistic basis for explaining how inter-cellular interactions influence cell fate determination, as indicated by recent experi-

ments, e.g., on the mouse ventral spinal cord [26], by allowing Notch to alter the expression of genes in the morphogen interpretation module, which in turn control the production of Notch ligands. Using a three-gene interpretation module associated with the Sonic Hedgehog (Shh) morphogen gradient in vertebrate neural tubes [34–36], we show that specific types of Notch-mediated coupling allow the size of the domains corresponding to different cell fates to be varied in a regulated manner. They retain the broad features of the reference pattern obtained in the absence of any intercellular coupling, while avoiding phenotypes that do not preserve the number and the sequence of these domains [Fig. 1 (a)]. Our results suggest that the emergent thresholds for the morphogen concentration that determine the localization of various cell fates are not only an outcome of the interaction between the morphogen gradient manifested across an entire embryonic segment with the gene circuit dynamics at the cellular level, but also the intermediate-scale dynamics of inter-cellular interactions.

To investigate how the spatial patterning of cell fates are affected by juxtacrine signaling, we consider a linear array of cells responding to a morphogen whose concentration decays exponentially away from the source [11, 37]. This spatial profile is reflected in the response of the cells in terms of the concentration of the downstream signaling molecules released as a result of binding of morphogen molecules to receptors on the cell membrane, viz.,  $S_M(x) = S_M(0)\exp(-x/\lambda_M)$ , where  $x$  is the distance of a cell from the source of the morphogen. The external signal concentration sensed by each cell through its receptors affects the expression of a set of genes that functions as the morphogen interpretation module. We choose one that has been proposed in the context of vertebrate neural tube patterning, comprising the genes Pax6, Olig2 and Nkx2.2, in the presence of a Sonic hedgehog (Shh) morphogen gradient [36]. Fig. 1 (b) shows the module with the regulatory motif of three patterning genes B, W and R, that mutually repress each other, with the sole exception of W by B. The gene having the highest expression level in each cell determines its fate, indicated

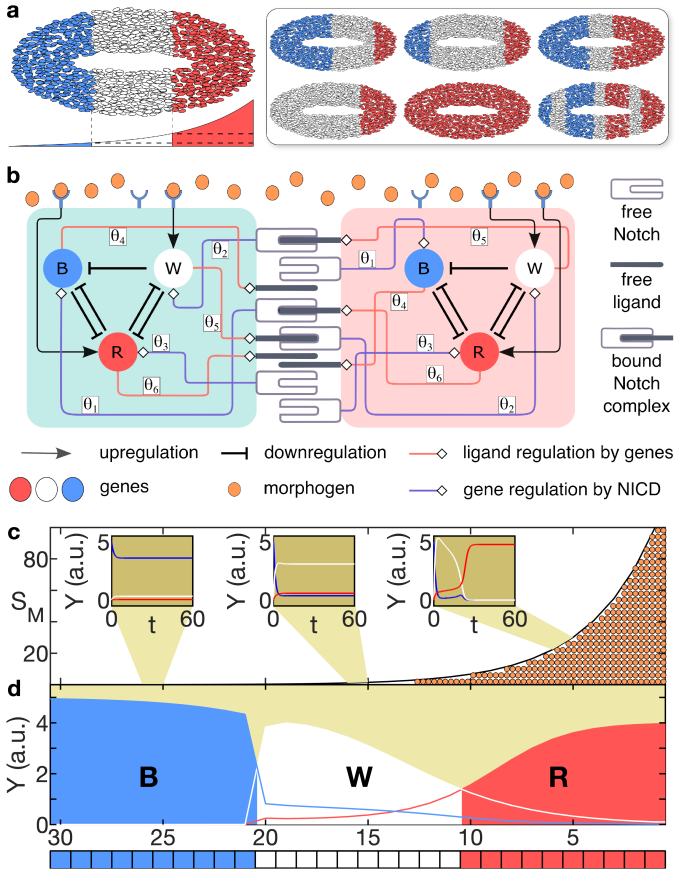


FIG. 1. **Contact-mediated signaling regulates the differential expression of cell fates dictated by morphogen concentration profiles.** (a) Schematic diagrams illustrating the French Flag problem, namely, how positional information provided by spatial gradients of morphogen concentration specify patterns of cell fates in embryonic tissue. Equally sized domains of cells exhibiting one of three different fates, viz., blue, white and red, characterize the idealized situation (left), shown for the case of patterning in the vertebrate neural tube by a gradient of Sonic hedgehog morphogen (whose concentration profile is displayed). Under different conditions, variations preserving the chromatic order and number of fate boundaries of the idealized situation can arise (a: right, top row); however, other variations may violate these (a: right, bottom row). (b) Schematic diagram of a pair of cells coupled via Notch signaling in the presence of an external morphogen. Each cell contains a morphogen interpretation module comprising a regulatory circuit of fate-inducing genes B, W and R. Notch intra-cellular domains (NICD), released upon successful binding of Notch receptors to ligands from the neighboring cell, affect expression of B, W and R with strengths  $\theta_{1,2,3}$ , respectively. This in turn regulates the production of Notch ligand with strengths  $\theta_{4,5,6}$ . (c) Spatial variation of the response  $S_M$  to the morphogen across a one-dimensional domain comprising 30 cells. The three insets display the time evolution of gene expression levels  $Y$  ( $= B, W$  or  $R$ , in arbitrary units) for cells that are subject to low, intermediate and high morphogen concentrations, respectively. (d) The resulting final expression levels  $Y$  of the patterning genes. The maximally expressed gene at each cell determines its fate, as shown in the schematic representation of the 1D domain displayed at the bottom.

by blue, white or red, which correspond to genes B, W and R, respectively [Fig. 1 (c-d)]. As Pax6 is the only gene whose expression occurs even in the absence of the Shh morphogen, we consider this pre-patterning gene (B) to be expressed at very high levels initially, in contrast to the other two. The time-evolution of the expression of the three genes are described by:

$$\frac{dB}{dt} = \frac{\alpha + \varphi_1 \frac{N^b}{K_N}}{1 + \left(\frac{R}{K}\right)^{h_1} + \left(\frac{W}{K}\right)^{h_2} + \xi_1 \frac{N^b}{K_N}} - k_1 B, \quad (1)$$

$$\frac{dW}{dt} = \frac{\beta S_M + \varphi_2 \frac{N^b}{K_N}}{1 + S_M + \xi_2 \frac{N^b}{K_N}} \frac{1}{1 + \left(\frac{R}{K}\right)^{h_3}} - k_2 W, \quad (2)$$

$$\frac{dR}{dt} = \frac{\gamma S_M + \varphi_3 \frac{N^b}{K_N}}{1 + S_M + \xi_3 \frac{N^b}{K_N}} \frac{1}{1 + \left(\frac{B}{K}\right)^{h_4} + \left(\frac{W}{K}\right)^{h_5}} - k_3 R, \quad (3)$$

where  $\alpha, \beta, \gamma$  are the maximum growth rates and  $k_{1,2,3}$  are the decay rates of expression for the three genes, while  $K, K_N$  and  $h_{1,2,3,4,5}$  specify the nature of the response functions. The parameters  $\varphi_{1,2,3}$  and  $\xi_{1,2,3}$  are associated with the juxtacrine coupling of adjacent cells through the canonical Notch signalling pathway [27, 28]. To describe the dynamics resulting from the coupling, Eqs. (1)-(3) are augmented with the time-evolution equations of the concentrations  $L$  and  $N^b$  of the Notch ligand and the Notch intra-cellular domain (NICD), respectively:

$$\frac{dL}{dt} = \frac{\beta_L + \phi_4 \frac{B}{K} + \phi_5 \frac{W}{K} + \phi_6 \frac{R}{K}}{1 + \zeta_4 \frac{B}{K} + \zeta_5 \frac{W}{K} + \zeta_6 \frac{R}{K}} - \frac{L}{\tau_L}, \quad (4)$$

$$\frac{dN^b}{dt} = \frac{\beta_{N^b} L^{trans}}{K + L^{trans}} - \frac{N^b}{\tau_{N^b}}. \quad (5)$$

Here, the parameters  $\beta_{L,N^b}$  and  $\tau_{L,N^b}$  correspond to the maximum growth rates and mean lifetimes for the ligand and NICD, respectively. The binding of Notch receptors of a cell to corresponding ligands of neighboring cells ( $L^{trans}$ ) causes the receptor's intracellular domain to be released and translocated to the nucleus [38]. We consider Notch and the patterning genes to regulate the expression of each other [see Fig. 1 (b)]. Specifically, we consider four classes of inter-cellular interactions based on whether NICD up or downregulates the expression of B, W and R genes, and whether Notch ligand production is promoted or repressed by the patterning genes (mirroring the response of the ligands Jagged and Delta, respectively [39–41]). For simplicity, the ligand is assumed to be either activated by all the genes or inhibited by each of them, while the genes themselves are regulated by NICD in a qualitatively identical manner. Thus, the four classes of inter-cellular coupling, defined by up ( $G^+$ ) or downregulation ( $G^-$ ) of the patterning genes, and promotion ( $L^+$ ) or repression ( $L^-$ ) of the ligand, and specified by the parameter set  $(\varphi_i, \xi_i, \phi_j, \zeta_j)$ , correspond to type I:  $G^-, L^-$  ( $0, \theta_i, 0, \theta_j$ ); type II:  $G^-, L^+$

$(0, \theta_i, \theta_j, 1)$ ; type III:  $G^+, L^- (\theta_i, 1, 0, \theta_j)$ ; and type IV:  $G^+, L^+ (\theta_i, 1, \theta_j, 1)$ , where  $i = 1, 2, 3$  and  $j = 4, 5, 6$ .

We choose values for the parameters such that the absence of coupling (i.e.,  $\varphi_i = 0$ ,  $\xi_i = 0$ ,  $\forall i$ ) yields an idealized flag with three chromatic regions of equal length, each corresponding to distinct cell fates (see SI). To see how Notch signalling between adjacent cells can alter the ordered pattern of cells having different fates, even when the morphogen gradient and the parameters of the interpretation module are kept unchanged, we systematically investigate the six-dimensional parameter space spanned by  $\Theta = \{\theta_1, \theta_2, \theta_3, \theta_4, \theta_5, \theta_6\}$ . For each of the four types of coupling described above, we consider  $10^5$  realizations of the model obtained by randomly sampling  $\Theta$ . Each of the parameters  $\theta_{1,\dots,6}$  is sampled from the interval  $[1, 10]$  (for  $G^+$  and  $L^+$ ) or  $[0.1, 1.0]$  (for  $G^-$  and  $L^-$ ). Altering the nature and strength of inter-cellular interactions, we observe a diversity of resulting patterns of distinct cell fates that differ from the flag obtained in the uncoupled case not only in terms of the lengths of the individual chromatic regions, but also in terms of their number and sequential order. To quantify the variation in the flags obtained from the different realizations, we characterize them by (i) the number  $n_B$  of fate boundaries, which are defined by adjacent cells having different fates, and (ii) a Hamming distance  $d_H$  to the idealized flag (obtained in the absence of coupling), determined by enumerating the number of cells whose fates are different in the two flags. Depending on whether NICD up or downregulates the expression of the patterning genes, we obtain two qualitatively different outcomes. While repression of B, W, R almost always results in flags having two boundaries [Fig. 2 (a-b)], promoting their expression yields a much wider range of  $n_B$  [Fig. 2 (c-d)]. Furthermore, the flags generated for coupling types I and II are typically closer (in terms of  $d_H$ ) to the idealized flag as compared to types III and IV.

In contrast to the parameters governing the regulation of B, W and R by NICD, those associated with modulating the effect of the patterning genes on ligand production appear to have little or no effect on the resulting flags. We use a variance-based sensitivity analysis technique to quantify the contribution of each of these parameters in determining the cell fates [1]. We consider the final state of each cell  $i$  comprising the domain to be represented by a discrete scalar variable  $F_i \in \{0, 1, 2\}$  corresponding to blue, white and red. Prior to quantifying the role played by the parameters  $\Theta$  at each cell, we quantify the variance ( $\sigma^2$ ) in the fate  $F_i$  across the different realizations [Fig. 3 (a-d), upper panels]. For coupling types I and II, we note that  $\sigma^2$  is negligible throughout the array, except around the location of the two fate boundaries in the idealized flag. In contrast,  $\sigma^2$  has a finite value at all locations in coupling types III and IV. The contribution of the different parameters  $\theta_{1,\dots,6}$  to the observed variation in the fate of each cell is measured by the respective first-

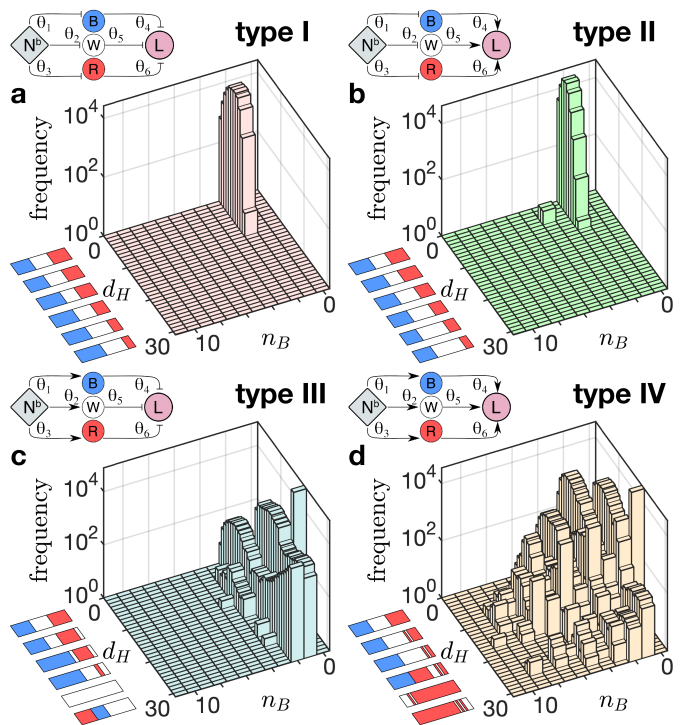


**FIG. 2. The diversity in the spatial patterns of cell fates is controlled by the nature of interactions underlying Notch-mediated inter-cellular coupling.** The inter-cellular interactions can be classified into four types, determined by whether NICD up or downregulates the patterning genes, and in turn, the genes up or downregulate ligand production, represented by the four motifs in the upper left corners in (a)-(d) [arrows representing up/downregulation are as indicated in Fig. 1 (b)]. For each type, the frequency distributions of different flags, i.e., patterns representing the sequential arrangement of distinct cell fates, are obtained by randomly sampling  $\theta_{1,\dots,6}$ , are shown in (a)-(d) for a 1D domain comprising 30 cells subject to the morphogen gradient shown in Fig. 1 (c). In the absence of inter-cellular coupling, the domain is divided into three equal segments of cells having different fates [as in Fig. 1 (d)]. The flags obtained upon coupling the cells are characterized by the number of fate boundaries  $n_B$  and the difference  $d_H$  with the pattern in the uncoupled system (which has equal chromatic divisions). For types I, II (where NICD downregulates B, W and R) almost all flags have the same chromatic order and  $n_B$  as the idealized flag shown in Fig. 1 (a, left), with  $d_H$  limited to very low values [a and b, cf. Fig. 1 (a, right, top row)]. In contrast, the flags seen for types III, IV (where NICD upregulates B, W and R) exhibit large variation from the uncoupled case in terms of both  $d_H$  and  $n_B$  [c and d, cf. Fig. 1 (a, right, bottom row)]. For each type, sample flags are displayed in ascending order of  $d_H$  along the corresponding axis.

order sensitivity indices  $S1$ , expressed as the variance of  $\langle F_i | \theta_j \rangle_{\theta_{k(\neq j)}}$  normalized by  $\sigma^2$  (see SI). Fig. 3 (a-d, lower panels) show that only  $\theta_2$  and  $\theta_3$  contribute significantly in all coupling types, while for coupling types III and IV,  $\theta_1$  also plays an important role. We note that the bulk of the variation in  $F_i$  can be explained by  $S1$  alone, suggest-

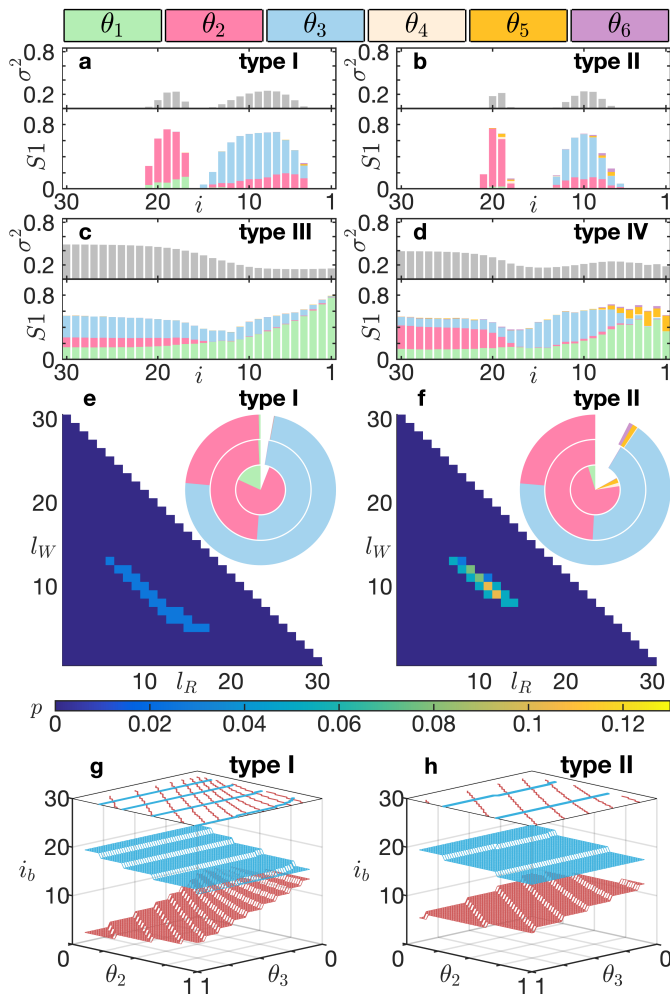


**FIG. 3. Sensitivity of the flags to inter-cellular coupling parameters.** (a-d) Dependence of the variation in cell fates on the spatial location of each cell in a 1D domain, as well as, the differential contributions of the coupling parameters  $\Theta$  to the variation, for the four types of Notch-mediated interactions. The top half of each panel shows the variance  $\sigma^2$  of the discrete variable representing the three possible fates (blue/white/red) that a cell can attain. The bottom halves display the fraction of the variance that can be accounted for by independently varying each of the parameters (colored according to the legend), as quantified by the first order sensitivity index  $S1$ . When NICD downregulates the patterning genes (a-b), most of the variation is localized around the two fate boundaries of the uncoupled case and is sensitive to changes in  $\theta_2$  and  $\theta_3$ . In contrast, variation is seen across the domain when NICD upregulates the genes (c-d), with most of the contribution from  $\theta_1$ ,  $\theta_2$  and  $\theta_3$ . (e-f) Focusing on types I, II for which chromatic order and  $n_B$  of the flags are invariant, we observe that the lengths of the red and white segments ( $l_R$  and  $l_W$ , respectively) are narrowly distributed around those in the uncoupled case ( $l_R^* = 10$ ,  $l_W^* = 10$ ). The sensitivity of the segment lengths to the parameters  $\Theta$  are shown in the concentric piecharts (outer:  $l_R$ , middle:  $l_W$ , inner:  $l_B$ ). (g-h) The dependence of the location  $i_b$  of the two fate boundaries (shown in blue and red, respectively) on the parameters  $\theta_2$  and  $\theta_3$ , with contour lines shown at the top.

ing that the observed diversity can be largely explained in terms of the independent actions of each parameter.

As flags that do not conserve  $n_B$  or the chromatic order of the idealized flag represent pronounced aberrations that are undesirable in the context of development, we focus on coupling types I and II that are extremely unlikely to generate such flags. Indeed, the localization of variation in cell fates for these coupling types is consistent with the resulting flags typically having low  $d_H$  (see Fig. 2). Moreover, almost all of them have  $n_B = 2$ , which allows the flags to be uniquely specified by the lengths of any two out of the three chromatic regions. Fig. 3 (e-f) shows that the joint distribution of the lengths  $l_R$ ,  $l_W$  of the regions having red and white fates, respectively, is concentrated around that of the flag obtained in absence of coupling (viz.,  $l_R = l_W = 10$  for an array of 30 cells) for both coupling types. The outer, middle and inner rings in the adjoining piecharts represent the contribution of each parameter  $\theta_{1,\dots,6}$  to the variation observed in  $l_R$ ,  $l_W$  and  $l_B$ , respectively. This is quantified by the corresponding first-order sensitivity indices, expressed in terms of the angles subtended by each of the colored segments representing the different parameters. Note that the bulk of the observed variance in the lengths can be attributed to changes in each of the parameters, independent of the others. As  $\theta_2$  and  $\theta_3$  appear to be almost exclusively responsible for the observed variation in the flags, in Fig. 3 (g-h) we explicitly show how the locations of the two boundaries  $i_b$  between R, W (red) and W, B (blue) change on varying these two parameters. For both coupling types, increasing  $\theta_2$  is observed to expand both the red and blue region at the expense of the white region in the middle, while increasing  $\theta_3$  results in reduction of the red region but with little impact on the W-B boundary. Thus, the variation in the flags resulting from down-regulation by NICD of the genes forming the morphogen interpretation module can be explained by using only a pair of parameters controlling the repression of W and R genes, respectively. The predicted alterations in the resulting flag upon changing Notch expression can be tested experimentally to validate the role of inter-cellular interactions in determining the spatial pattern of cell fates outlined here.

To conclude, our work reveals that juxtacrine signaling between cells could play a key role in adaptively regulating cellular differentiation that results in morphogenesis. While the diffusing morphogen, by setting up a global field acts as the signal triggering the breaking of the intrinsic symmetry, and the gene regulatory circuit forming the interpretation module translates the local morphogen concentration into the eventual cell fates, inter-cellular interactions allow the information from the environment of each cell to be incorporated into the process. Apart from their utility in correcting for fluctuations in the signal in the presence of noise [29], such an intermediate-scale process can increase the robustness of

the system in generating the desired flag by compensating for mutations affecting the production and/or interpretation of the morphogen. We show this by using a modeling approach that integrates two apparently disparate paradigms for investigating biological pattern formation [31], namely, that of boundary-organized mechanisms involving a pre-pattern such as a morphogen concentration gradient, and self-organized mechanisms involving interactions between constituents [43].

We would like to thank James P. Sethna for helpful discussions. SNM has been supported by the IMSc Complex Systems Project (12th Plan), and the Center of Excellence in Complex Systems and Data Science, both funded by the Department of Atomic Energy, Government of India. The simulations required for this work were supported by IMSc High Performance Computing facility (hpc.imsc.res.in) [Nandadevi].

- 
- [1] M. C. Cross and P. C. Hohenberg, *Rev. Mod. Phys.* **65**, 851 (1993). doi:10.1103/RevModPhys.65.851
- [2] A. J. Koch and H. Meinhardt, *Rev. Mod. Phys.* **66**, 1481 (1994). doi:10.1103/RevModPhys.66.1481
- [3] P. Ball, *The Self-made Tapestry: Pattern Formation in Nature* (Oxford University Press, Oxford, 1999). doi:10.1119/1.880339
- [4] H. T. Zhang and T. Hiiragi, *Annu. Rev. Cell Dev. Biol.* **34**, 405 (2018). doi:10.1146/annurev-cellbio-100617-062616
- [5] A. M. Turing, *Philos. Trans. R. Soc. B* **237**, 37 (1952). doi:10.1098/rstb.1952.0012
- [6] H. Meinhardt, *Models of Biological Pattern Formation* (Academic Press, London, 1982).
- [7] S. Werner, T. Stückemann, M. B. Amigo, J. C. Rink, F. Jülicher, and B. M. Friedrich, *Phys. Rev. Lett.* **114**, 138101 (2015). doi:10.1103/PhysRevLett.114.138101
- [8] L. Wolpert, *J. Theor. Biol.* **25**, 1 (1969). doi:10.1016/s0022-5193(69)80016-0
- [9] L. Wolpert, *Development* **107**, 3 (1989). doi:10.1016/j.jtbi.2010.10.034
- [10] J. Sharpe, *Development*, **146**, dev185967 (2019). doi:10.1242/dev.185967
- [11] F. Crick, *Nature (Lond.)* **225**, 420 (1970). doi:10.1038/225420a0
- [12] W. Driever and C. Nüsslein-Volhard, *Cell* **54**, 95 (1988). doi:10.1016/0092-8674(88)90183-3
- [13] A. A. Teleman, M. Strigini, and S. M. Cohen, *Cell* **105**, 559 (2001). doi:10.1016/s0092-8674(01)00377-4
- [14] A. D. Lander, Q. Nie, and F. Y. M. Wan, *Dev. Cell* **2**, 785 (2002). doi:10.1016/s1534-5807(02)00179-x
- [15] A. D. Lander, *Cell* **128**, 245 (2007). doi:10.1016/j.cell.2007.01.004
- [16] T. Bollenbach, K. Kruse, P. Pantazis, M. González-Gaitán, and F. Jülicher, *Phys. Rev. Lett.* **94**, 018103 (2005). doi:10.1103/physrevlett.94.018103
- [17] J. L. England and J. Cardy, *Phys. Rev. Lett.* **94**, 078101 (2005). doi:10.1103/physrevlett.94.078101
- [18] G. Hornung, B. Berkowitz, and N. Barkai, *Phys. Rev. E* **72**, 041916 (2005). doi:10.1103/physreve.72.041916
- [19] D. Ben-Zvi and N. Barkai, *Proc. Natl. Acad. Sci. USA* **107**, 6924 (2010). doi:10.1073/pnas.0912734107
- [20] S. B. Yuste, E. Abad, and K. Lindenberg, *Phys. Rev. E* **82**, 061123 (2010). doi:10.1103/physreve.82.061123
- [21] C. B. Muratov, P. V. Gordon, and S. Y. Shvartsman, *Phys. Rev. E* **84**, 041916 (2011). doi:doi.org/10.1103/physreve.84.041916
- [22] J. B. Gurdon and P-Y. Bourillot, *Nature (Lond.)* **413**, 797 (2001). doi:10.1038/35101500
- [23] H. L. Ashe and J. Briscoe, *Development* **133**, 385 (2006). doi:10.1242/dev.02238
- [24] K. W. Rogers and A. F. Schier, *Annu. Rev. Cell Dev. Biol.* **27**, 377 (2011). doi:10.1146/annurev-cellbio-092910-154148
- [25] S. F. Gilbert, *Developmental Biology* (Sinauer, Sunderland, MA, 2013).
- [26] J. H. Kong, L. Yang, E. Dessaud, K. Chuang, D. M. Moore, R. Rohatgi, J. Briscoe, and B. G. Novitch, *Dev. Cell* **33**, 373 (2015). doi:10.1016/j.devcel.2015.03.005
- [27] S. Artavanis-Tsakonas, M. D. Rand, and R. J. Lake, *Science* **284**, 770 (1999). doi:10.1126/science.284.5415.770
- [28] R. Kopan and M. X. G. Ilagan, *Cell* **137**, 216 (2009). doi:10.1016/j.cell.2009.03.045
- [29] D. Sprinzak, A. Lakhanpal, L. LeBon, J. Garcia-Ojalvo, and M. B. Elowitz, *PLoS Comput. Biol.* **7**, e1002069 (2011). doi:10.1371/journal.pcbi.1002069
- [30] T. Erdmann, M. Howard, and P. R. Ten Wolde, *Phys. Rev. Lett.* **103**, 258101 (2009). doi:10.1103/physrevlett.103.258101
- [31] A. D. Lander, *Cell* **144**, 955 (2011). doi:10.1016/j.cell.2011.03.009
- [32] A. D. Lander, *Science* **339**, 923 (2013). doi:10.1126/science.1224186
- [33] The feedback loop arises from the Notch intra-cellular domain (NICD) of a cell  $i$  controlling the production of NICD in the neighboring cell  $j$  by affecting the production of the corresponding ligand in cell  $i$ , which in turn results in NICD of  $j$  controlling that of  $i$ , thereby completing the loop.
- [34] E. Dessaud, A. P. McMahon, and J. Briscoe, *Development* **135**, 2489 (2008). doi:doi.org/10.1242/dev.009324
- [35] E. Dessaud, V. Ribes, N. Balaskas, L. L. Yang, A. Pierani, A. Kicheva, B. G. Novitch, J. Briscoe, and N. Sasai, *PLoS Biol.* **8**, e1000382 (2010). doi:10.1371/journal.pbio.1000382
- [36] N. Balaskas, A. Ribeiro, J. Panovska, E. Dessaud, N. Sasai, K. M. Page, J. Briscoe, and V. Ribes, *Cell* **148**, 273 (2012). doi:doi.org/10.1016/j.cell.2011.10.047
- [37] We assume that the concentration of morphogens across the domain is implicitly set by a spatially uniform linear synthesis-diffusion-degradation (SDD) model, which yields an exponential gradient in the morphogen concentration  $M$  at its steady state. We assume that  $S_M$  is a proxy for the concentration of the signaling molecule that is triggered when morphogen molecules bind successfully with the cell membrane receptors.
- [38] We assume the number of receptors in each cell to be sufficiently high such that saturation is not reached.
- [39] H. Shimojo, T. Ohtsuka, and R. Kageyama, *Front. Neurosci.* **5**, 78 (2011). doi:10.3389/fnins.2011.00078
- [40] L. J. Manderfield, F. A. High, K. A. Engleka, F. Liu, L. Li, S. Rentschler, and J. A. Epstein, *Circulation* **125**, 323 (2012). doi:10.1161/circulationaha.111.047159
- [41] M. Boareto, M. K. Jolly, M. Lu, J. N. Onuchic, C. Clementi, and E. Ben-Jacob, *Proc. Natl. Acad. Sci. USA*

**112**, E402 (2015). doi:10.1073/pnas.1416287112

[42] A. Saltelli and I. M. Sobol, *Matem. Mod.* **7**, 16 (1995).

[43] J. B. A. Green and J. Sharpe, *Development* **142**, 1203 (2015). doi:10.1242/dev.114991

## SUPPLEMENTARY INFORMATION

### Contact-mediated cellular communication supplements positional information to regulate spatial patterning during development

Chandrashekar Kuyyamudi, Shakti N. Menon and Sitabhra Sinha

#### LIST OF SUPPLEMENTARY FIGURES

1. Fig S1: The final expression levels  $B$ ,  $W$  and  $R$  of the patterning genes, as well as, the concentrations of the Notch ligand,  $L$ , and NICD,  $N^b$ , for each of the coupling types..
2. Fig S2: Spatio-temporal evolution of the expression levels of the patterning genes B, W, and R at different cells in a 1D array comprising 30 cells.
3. Fig S3: The effect of differential expression of Notch on cell fates.
4. Fig S4: ‘‘Sloppy parameter sensitivity’’ of the flags to inter-cellular coupling.

#### MODEL PARAMETER VALUES

parameter	$S_M(0)$	$\lambda_M$	$\alpha$	$\beta$	$\gamma$	$\beta_L$	$\beta_{N^b}$	$K$	$K_N$	$k_1$	$k_2$	$k_3$	$\tau_L$	$\tau_{N^b}$	$h_1$	$h_2$	$h_3$	$h_4$	$h_5$
value	100.0	0.3	4.0	6.3	5.0	5.0	5.0	1.0	1.0	1.0	1.0	1.0	1.0	1.0	6	2	5	1	1

TABLE S1. The values for the model parameters used for all simulation results reported (unless specified otherwise).

#### TEMPORAL EVOLUTION AND PARAMETER DEPENDENCE OF THE PATTERNS REPRESENTING THE SEQUENTIAL ARRANGEMENT OF DISTINCT CELL FATES

The fate of each cell in the linear array we consider in our simulation is determined by the expression levels of the three patterning genes B, W and R at  $t_{max} = 100$ . Gene B is chosen to be the pre-patterning gene, such that its expression level is high (= 5 arb. units) initially while the initial expression level of the genes W and R is 0. Fig. S1 shows for each of the coupling types considered in the main text, the time evolution of the expression levels for B, W and R with a representative set of values chosen for the coupling parameters. For coupling types I and II, B continues to be the maximally expressed gene in cells that have relatively low exposure to the morphogen, while in cells subject to intermediate and high morphogen concentrations W and R genes (respectively) are the maximally expressed ones. In case of types III and IV, more than two fate boundaries can emerge and the chromatic order seen in the uncoupled system is not conserved. This implies that the coupling types III and IV give rise to a large diversity of flags, compared to types I and II.

Fig. S2 shows the final expression levels of the three patterning genes B, W, R in all the cells of the linear array, along with the concentrations of the Notch ligand,  $L$ , and the Notch intra-cellular domain NICD,  $N^b$ , for four representative sets of parameter values for each of the four coupling types.

We have considered the maximal production rate of NICD,  $\beta^{N^b}$  to be 5 for all the results described in the main text. To understand the implications of the over or under-expression of Notch for the results of our model, we have also performed simulations by considering a wide range of values of  $\beta^{N^b}$ . We consider only coupling types I and II which conserve the number of boundaries and the chromatic order observed in the uncoupled system, ensuring that pathological patterns of cell fates do not arise for  $\beta^{N^b} = 5$ . Fig. S3 shows the variation in length of the chromatic regions as a function of  $\beta^{N^b}$  for four different sets of coupling parameter values for each of the two coupling types. It is evident that, depending on the values of the coupling parameters chosen, the higher expression of Notch can lead to either increase or reduction of the red region, while the width of the blue region remains largely invariant. This result suggests that experimental observation of the effect of under or over-expression of Notch on the length of the regions with different cell fates can provide us with information about the type of coupling and the strength of interactions in different biological systems.

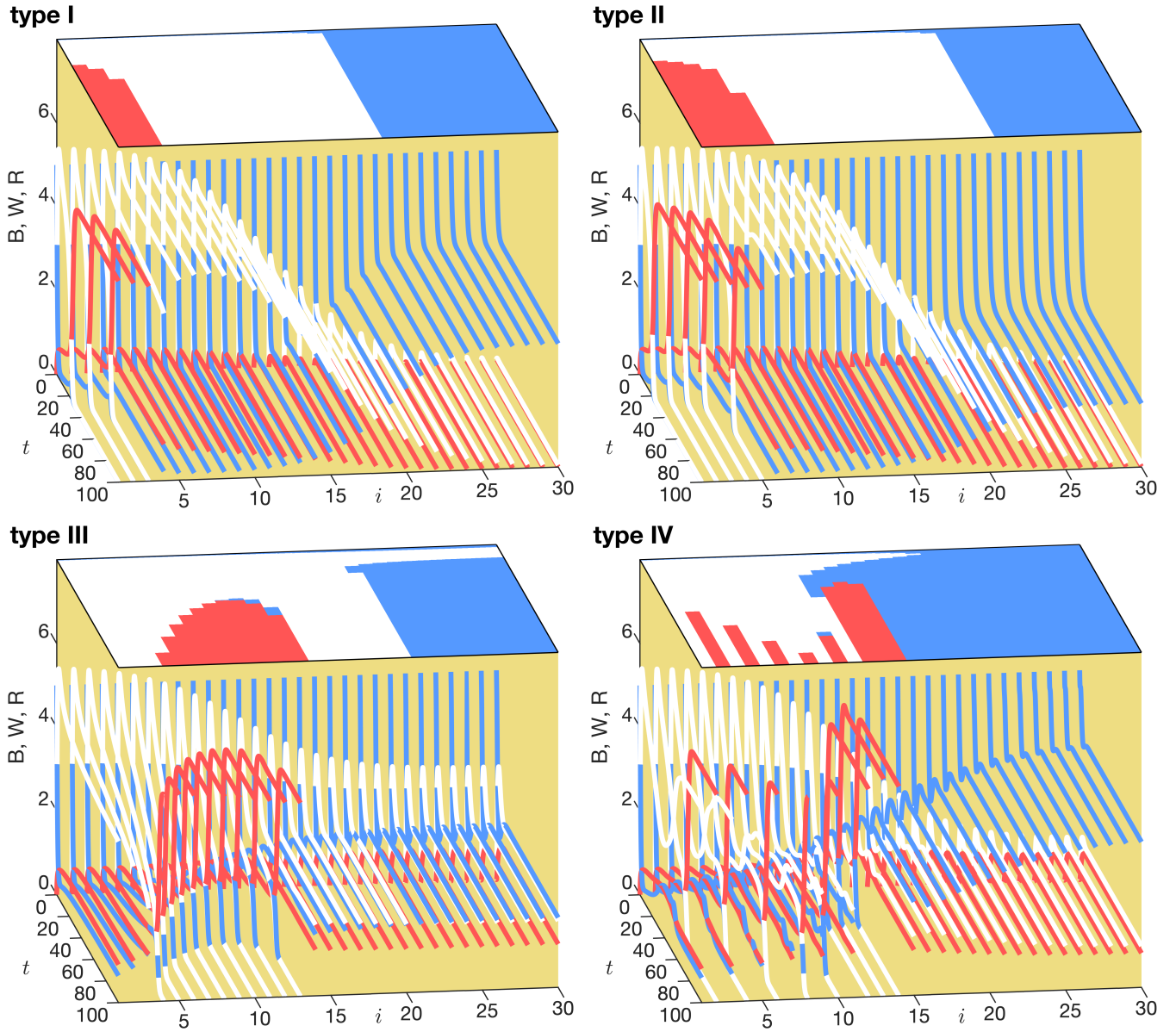


FIG. S1. Spatio-temporal evolution of the expression levels of the patterning genes **B**, **W**, and **R** at different cells in a 1D array comprising 30 cells. The resulting cell fates are indicated on the top surface of each panel corresponding to the coupling types I-IV. For each coupling type, a representative parameter set  $\Theta$  is used for the simulation. Note that, all cells initially exhibit high expression levels for B.



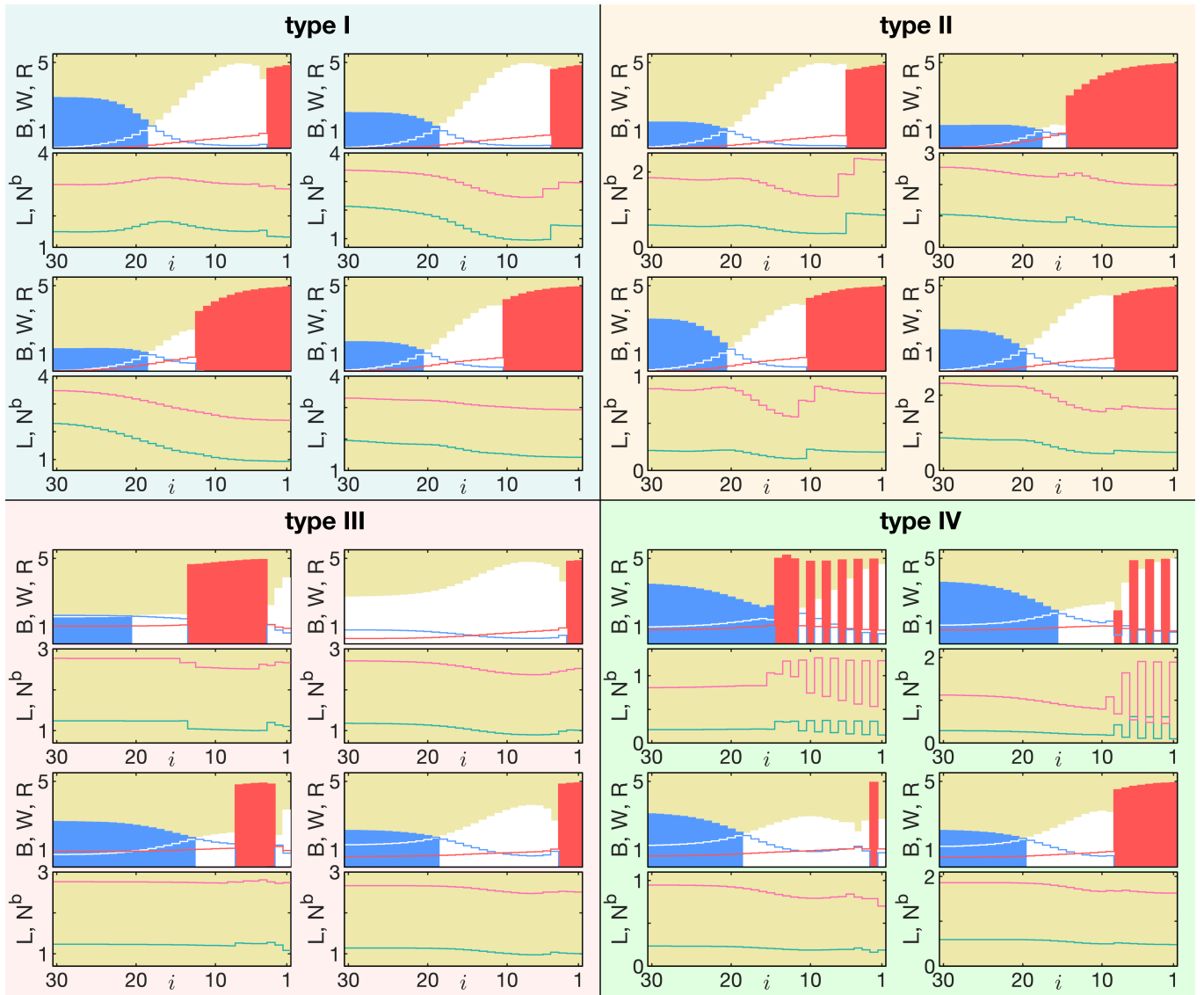


FIG. S2. The final expression levels  $B$ ,  $W$  and  $R$  of the patterning genes, as well as, the concentrations of the Notch ligand,  $L$ , and NICD,  $N^b$ , for each of the coupling types. The maximally expressed gene at each cell in the 1D array determines its fate, indicated by the colors blue, white or red. For each coupling type, results obtained using different choices of values for the parameter set  $\Theta$  are shown.

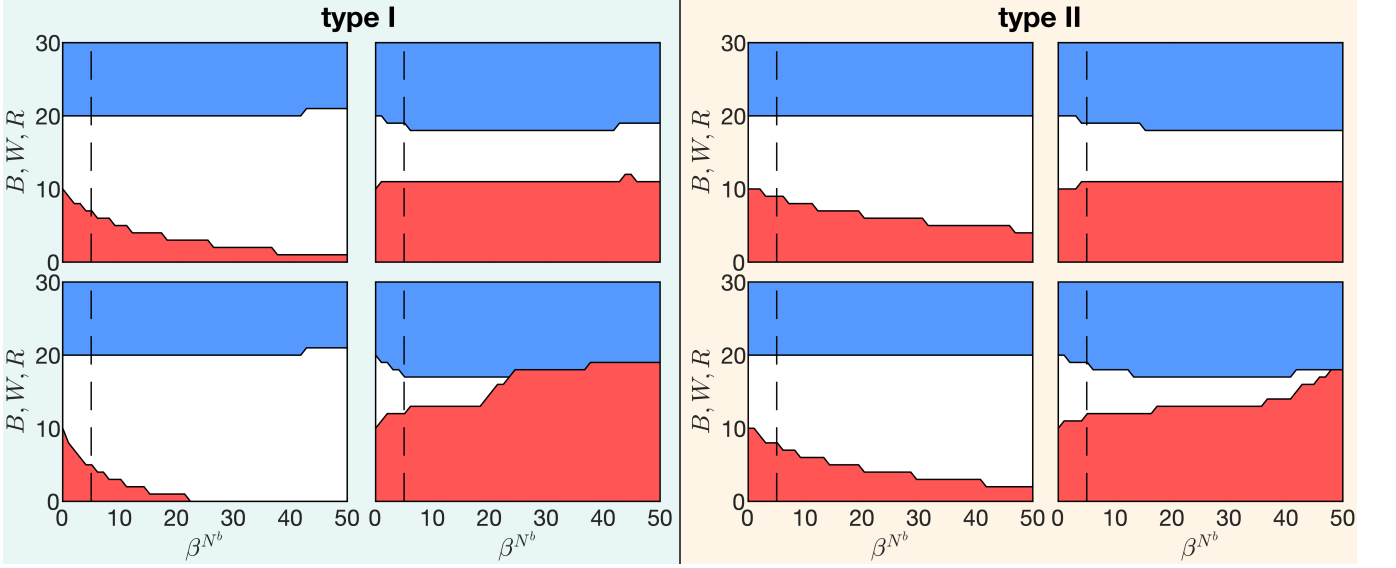


FIG. S3. **The effect of differential expression of Notch on cell fates.** The variation of the spatial extent of the three chromatic regions (indicated using the colors blue, white and red) with the NICD maximal production rate,  $\beta^{N^b}$ , for coupling types I and II which preserve the chromatic order and number of boundaries seen in the uncoupled system. For all results shown in the main text, we have chosen  $\beta^{N^b} = 5$  (indicated using a broken line). The result of under or over-expression of Notch relative to this value is shown for different choices of values for the parameter set  $\Theta$  in the case of each coupling type.

## PARAMETER SENSITIVITY

### Variance-based sensitivity analysis

To quantify the contribution of the parameters governing the regulation of the patterning genes by NICD in determining the cell fates, we have used a variance-based sensitivity analysis often referred to as the Sobol method [1]. This method can be used to investigate the effect of varying any one of the parameters, or a pair of them at a time, or any other higher-order combinations. We consider a system that yields a scalar output as a function of parameters  $\theta_j$ ,

$$Y = f(\theta_1, \theta_2, \dots, \theta_k). \quad (6)$$

The first-order sensitivity index, which corresponds to the fraction of the total variation in  $Y$  that can be attributed to varying only  $\theta_j$ , keeping the other parameters fixed, is defined as

$$S1(j) = \frac{V_{\theta_j}(E_{\theta_{-j}}(Y|\theta_j))}{V(Y)}. \quad (7)$$

Here,  $-j$  refers to all other parameters except  $j$ . For each cell this sensitivity index is, by definition, bound within the range  $0 \leq S1(j) \leq 1$ . Note that the fraction of the total variance in the output variable that can be explained by changing one parameter at a time is given by the sum over all the first-order sensitivity indices,  $\sum_j S1(j) \leq 1$ .

As mentioned in the main text, we quantitatively investigate the role of the parameter set  $\Theta$  in determining the final state of the cells  $i$  ( $i = 1, \dots, 30$ ) represented by a discrete scalar variable,  $F_i \in \{0, 1, 2\}$ . The contribution of each of  $\theta_k$  ( $k = 1, \dots, 6$ ) to the observed variation in cell fates is measured by the respective first-order sensitivity indices  $S1$ , expressed as the variance of  $\langle F_i|\theta_j \rangle_{\theta_{k(\neq j)}}$  normalized by  $\sigma^2$  ( $i = 1, \dots, 30$ ). In case of the coupling types I and II, we almost always observe two boundaries separating the distinct regions. This allows us to uniquely identify a resultant flag by specifying  $l_R$ ,  $l_W$  and  $l_B$ , which correspond to the lengths of the red, white and blue regions, respectively, and which can take discrete values in the range  $[0, 30]$ . Corresponding to these three scalar variables, we obtain first-order sensitivity indices  $S1^R$ ,  $S1^W$  and  $S1^B$ , using quasi Monte Carlo methods.

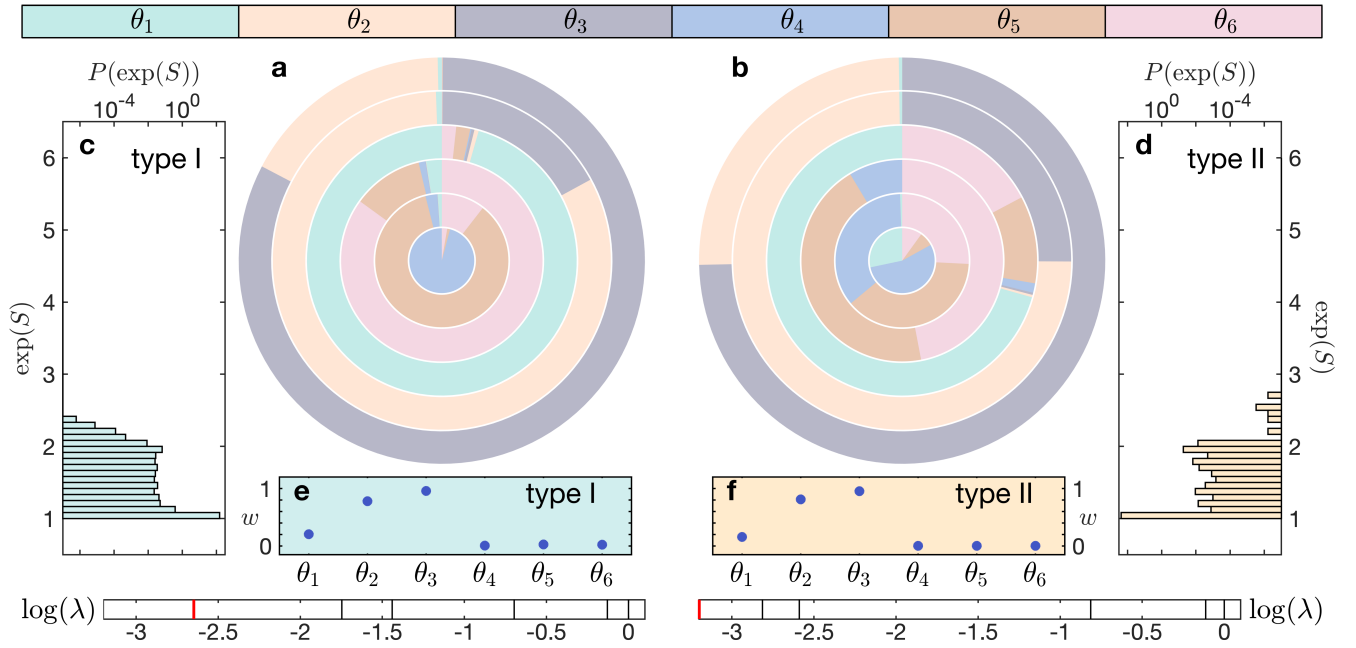


FIG. S4. “Sloppy parameter sensitivity” of the flags to inter-cellular coupling. The concentric pie charts (a: type I, b: type II) show the fractional contribution of the components of the parameter set  $\Theta$ , represented by colors indicated in the key at the top, to the sensitivity of the system to parameter variation. This is expressed in terms of the spectral characteristics of the Hessian matrix, whose eigenvalues  $\lambda$  obtained for a specific parameter set for each coupling type are shown at the bottom. For both coupling types, the two largest eigenvalues are comparable in magnitude while there is a large gap between these and the subsequent eigenvalues. The bar plots (c: type I, d: type II) show the probability distribution [in logarithmic scale] of the exponential function of entropy  $S$  for the eigenvector components of the Hessian calculated for an ensemble of  $10^3$  randomly chosen parameter sets  $\Theta$ . Note that, as  $\exp(S)$  provides a measure for the number of dominant components in an eigenvector, most eigenvectors are dominated by a single component. This is in agreement with the observation that almost all of the concentric shells in the pie charts show the predominance of one color. The aggregated contribution  $w$  of each parameter to the eigenvectors (e: type I, f: type II) indicates that, consistent with the variance-based sensitivity analysis reported in the main text,  $\theta_2$  and  $\theta_3$  are almost exclusively responsible for the observed variation in the flags.

### “Sloppy parameter sensitivity” analysis

As a supplement to the variance-based sensitivity analysis, we have characterized the sensitivity of the model output to variation of the parameters  $\Theta = \{\theta_1, \dots, \theta_6\}$  using “sloppy model analysis” [2–4].

This is done by varying each parameter over a relevant range and calculating a Jacobian matrix that captures the variation of output variables of interest. The Jacobian is then used to obtain a Hessian matrix whose spectrum indicates the sensitivity of the system to each of the parameters.

The output variables that we use to characterize the sloppiness of the model are the lengths of the blue, white and red regions. These are specified using the 3-tuple  $(B, W, R)$ , each of which can take integer values between 0 and 30, subject to the constraint that  $B + W + R = 30$ . In conventional sloppy analysis of models, a specific set of parameter values is chosen as the reference set  $\Theta^*$  and the results of variations from this set are then investigated. As in our model, there is no such privileged parameter set, we have carried out the analysis using several different  $\Theta^*$  obtained by randomly choosing values of each of the parameters from their respective ranges.

To quantify the sloppiness of our model system, we compare the lengths of the regions  $(B^*, W^*, R^*)$  obtained using a given set  $\Theta^*$  with those obtained using perturbed parameter sets. Each perturbed set  $\Theta_{i,j}$  is obtained by independently varying the value of the parameter  $\theta_j$  in the set  $\Theta^*$  over the relevant range in small steps of  $\Delta\theta$ , while keeping values of the other five parameters fixed. Thus, for a given choice of  $\Theta^*$  and  $\Theta_{i,j}$ , the residue is

$$\mathcal{R}_{i,j} = \sqrt{(B_{i,j} - B^*)^2 + (W_{i,j} - W^*)^2 + (R_{i,j} - R^*)^2}, \quad (8)$$

where  $(B_{i,j}, W_{i,j}, R_{i,j})$  denotes the lengths of the regions obtained using the parameter set  $\Theta_{i,j}$ . This is then used to obtain the Jacobian matrix  $\mathbf{J}$  as

$$J_{i,j} = \frac{\mathcal{R}_{i+1,j} - \mathcal{R}_{i,j}}{\Delta\theta}, \quad (9)$$

which comprises  $(k - 1)$  rows and 6 columns, where  $k$  is the number of perturbed parameter sets considered. This subsequently yields the  $6 \times 6$  Hessian matrix

$$\mathcal{H} = J^T J. \quad (10)$$

We calculate the eigen spectrum of  $\mathcal{H}$  and normalize the eigenvalues by the largest eigenvalue. The number of “sloppy” directions corresponds to the number of eigenvalues whose normalized magnitude  $\ll 1$ . The eigenvector corresponding to an eigenvalue whose magnitude is very small represents an axis in the 6-dimensional parameter space along which any variation has relatively little impact on the output. Our results indicate that most eigenvectors have a single large component.

We obtain the Hessian spectra for each of  $10^3$  different random choices of  $\Theta^*$  (Fig. S4). Using these, we establish a hierarchy of the six parameters  $\theta_j$  in terms of their “weights” defined as

$$w_{\theta_j} = \frac{1}{N_{\Theta^*}} \sum_{\Theta^*} \sum_{k=1}^6 \lambda^k v_{\theta_j}^k * v_{\theta_j}^k, \quad (11)$$

where the first summation is over all  $10^3$  parameter sets  $\Theta^*$  and the second is over the six components of the spectra of  $\mathcal{H}$ . Further,  $\lambda^k$  and  $v_{\theta_j}^k$  are the eigenvalue and eigenvector of the  $k$ -th component of the Hessian spectra obtained upon varying the parameter  $\theta_j$ .

- 
- [1] A. Saltelli and I. M. Sobol, *Matem. Mod.* **7**, 16 (1995).  
[2] K. S. Brown and J. P. Sethna, *Phys. Rev. E* **68**, 021904 (2003). doi:10.1103/physreve.68.021904  
[3] J. J. Waterfall, F. P. Casey, R. N. Gutenkunst, K. S. Brown, C. R. Myers, P. W. Brouwer, V. Elser and J. P. Sethna *Phys. Rev. Lett.* **97**, 150601 (2006). doi:10.1103/physrevlett.97.150601  
[4] R. N. Gutenkunst, J. J. Waterfall, F. P. Casey, K. S. Brown, C. R. Myers and J. P. Sethna *PLoS Comput. Biol.* **3**, e189 (2007). doi:10.1371/journal.pcbi.0030189.eor